The fabrication, characterization and electrochemical corrosion behavior of Zn-TiO_2 composite coatings

Phys. Scr. **84** (2011) 035601 (10pp) doi:10.1088/0031-8949/84/03/035601

The fabrication, characterization and electrochemical corrosion behavior of Zn-TiO_2 composite coatings

M K Punith Kumar[1], T V Venkatesha[1], M K Pavithra[1] and A Nithyananda Shetty[2]

[1] Department of PG Studies and Research in Chemistry, Kuvempu University, Shankaraghatta 577 451, India
[2] Department of Chemistry, National Institute of Technology Karnataka, Surathkal 575 025, India

E-mail: drtvvenkatesha@yahoo.co.uk

Received 28 April 2011
Accepted for publication 14 July 2011
Published 4 August 2011
Online at stacks.iop.org/PhysScr/84/035601

Abstract
Metal-nanoparticle composite coatings improve the hardness, wear resistance and corrosion resistance properties of metal coatings. In this work, TiO_2 nanoparticles were chosen as second-phase particles to generate anticorrosive Zn composite coatings. The TiO_2 nanoparticles were dispersed in a Zn plating solution to co-deposit them with Zn. The Zn-TiO_2 composite coatings were then characterized by scanning electron microscopy (SEM), energy-dispersive x-ray spectroscopy (EDS) and x-ray diffraction methods. The presence of TiO_2 particles in the composite was confirmed by SEM images and EDS spectra. The Zn-TiO_2 composite coatings incorporated with different amounts of TiO_2 particles were tested for corrosion performance by polarization and electrochemical impedance spectroscopy, and the dissolution behavior of the coatings that had been immersed in corrosive media for a long time was studied. Improved corrosion resistance properties of the Zn-TiO_2 composite coatings were confirmed by polarization studies, fitted Nyquist plots, an increase in phase angle and a shift in the R_{ct} characteristic peak of the Bode plot.

PACS numbers: 68.55.jm, 68.37.HK, 81.15.−Z, 81.65.Kn, 82.45.Bb, 82.80.Fk, 84.37.+q

(Some figures in this article are in colour only in the electronic version.)

1. Introduction

Mild steel has found wide applications in industry and machinery because of its cost and potential properties. However, it is highly susceptible to corrosion and complete protection against corrosion has always been a challenge to researchers [1]. Among various corrosion control methods, Zn deposition is extensively used for protecting steel from corrosion because of its sacrificial nature, but Zn itself undergoes corrosion by forming white rust-like precuts on its surface. Hence, a possible solution to this problem is the fabrication of a Zn-nanoparticle composite coating on the steel, instead of the environmentally hazardous post-plating treatments of Zn coating such as chrome passivation and surface modification with organic chelating agents [2]. Comparatively, Zn composite coatings provide superior mechanical properties and better protection of the steel than a pure Zn coating, since they corrode at a slower rate than pure Zn.

The fabrication of metal-particle composites can be achieved by various methods such as electrodeposition, electroless plating, hot dipping, chemical and physical vapor deposition, stir casting and plasma spraying techniques. Of these methods, electrodeposition has advantages like low cost, room-temperature operation, single step, good reproducibility and less pollution [3–5]. The second-phase particles used in metal composite coatings are oxides, nitrides or carbides of different metals. A variety of nanosized particles have been successfully co-deposited with several metals. To obtain composite films the metal deposit, incorporated with ZrO_2 [6],

Table 1. Optimized bath composition and operating parameters for zinc deposition.

Bath composition	Concentration	Operating conditions
$ZnSO_4$	180 g l^{-1}	Anode, zinc plate (99.99% pure)
Na_2SO_4	30 g l^{-1}	Cathode, mild steel plate
NaCl	10 g l^{-1}	Current density, 0.03 A cm^{-2}
SLS (sodium lauryl sulfate)	1.5 mM	Plating time, 10 min Stirring speed, 400 rpm pH, 2.5; temperature, 27 ± 2 °C

WC (tungsten carbide) [2], TiO_2 [5], Al_2O_3 [4, 7] and SiC [8] particles, shows higher wear resistance with hardness, and the carbon nanotube (CNT) [9], Al_2O_3 [7], TiO_2 [10], SnO_x [11] and SiO_2 [12] particles provide a high corrosion resistance property to the composite. In addition, the incorporation of particles such as MoS_2, graphite and PTFE (polytetrafluoroethylene) into the metal matrix provides greater self-lubrication [12, 13].

Nanosized TiO_2 particles are in great demand for the generation of composite metal coatings because they exhibit properties such as photo-induced biocidal effects, wear and corrosion resistance, and are semiconducting and photocatalytic [10], [14–17]. The Zn-TiO_2 metal matrix predominantly shows higher corrosion resistance due to considerable morphological changes in the deposit [10].

In the literature, few results on the fabrication and corrosion behavior of Zn-TiO_2 composite coatings using different types and different sized TiO_2 nanoparticles were reported. Vlasa *et al* [18] reported on the corrosion behavior of Zn-TiO_2 composites by taking 32 nm anatase and Degussa TiO_2 nanoparticles. They studied the corrosion behavior of composite coatings up to 48 h and analyzed it on the basis of fitted Nyquist plots.

In most of the studies, authors selected a single concentration of nanoparticles in a bath to generate a composite coating and measured its properties along with the corrosion behavior. Therefore, the present work is directed towards fabricating a Zn-TiO_2 composite from solutions containing different concentrations of $\leqslant$ 25 nm anatase TiO_2 nanoparticles. The Zn-TiO_2 composite coatings were characterized by scanning electron microscopy (SEM), energy-dispersive x-ray spectroscopy (EDS) and x-ray diffraction (XRD) studies. The corrosion performance of the Zn-TiO_2 composite coating was tested using Tafel plots, linear polarization, and predominantly the impedance method (EIS; electrochemical impedance spectroscopy). In EIS, the corrosion behavior of the coatings was analyzed on the basis of fitted Nyquist plots and variation of phase angle with R_{ct} characteristic peaks of Bode plots up to 72 h.

2. Experimental procedure

Zn-TiO_2 composite coatings were generated on a mild steel specimen from the Zn plating bath (table 1), which contained suspended TiO_2 nanoparticles. Anatase TiO_2 nanoparticles ($\leqslant$ 25 nm (637254–50 g, batch number MKAA1560)) purchased from Sigma Aldrich, India, and other chemicals of analytical grade purchased from Himedia, India, were used.

The plating solutions were prepared by adding 2, 6 and 10 g l^{-1} of anatase TiO_2 nanoparticles and were then stirred for 24 h by a magnetic stirrer (Remi) to ensure the uniform dispersion of nanoparticles in the plating solution. For the plating process, mild steel (AISI 1079, composition $C = 0.5$, Mn = 0.5, $S = 0.005$ and Fe = 98.95%) with an area of 4 × 4 cm^2 and a Zn metal plate with the same dimensions were used as the cathode and anode, respectively. The mild steel plates were polished mechanically and degreased with trichloroethylene in a degreaser plant, followed by a water wash. The plates were then dipped in 10% HCl to remove rust and rinsed in water. The Zn plate surface was activated by dipping it in 5% HCl for a few seconds, followed by a water wash.

The electrodeposition process was carried out at a current density of 0.03 A cm^{-2} for 10 min with a solution stirring speed of 400 rpm at 27 ± 2 °C. The obtained coatings were named as P_0 (Zn + 0 g l^{-1} TiO_2), P_1 (Zn + 2 g l^{-1} TiO_2), P_2 (Zn + 6 g l^{-1} TiO_2) and P_3 (Zn + 10 g l^{-1} TiO_2).

The surface morphology of the coating was investigated using a JOEL–JEM–1200–EX II SEM, and the TiO_2 particle content in the coated film was determined by EDS analysis coupled with SEM. XRD analysis of the electrodeposits was carried out using a Philips TW3710 x-ray diffractometer with Cu $K\alpha$ radiation ($\lambda = 0.1540$ nm), working at 30 mA and 40 kV.

The electrochemical corrosion studies were performed in a conventional glass cell using a CHI 660C electrochemical work station (United State) at 27 ± 2 °C. The Zn and Zn-TiO_2 coated steel specimen, a platinum wire and a saturated calomel electrode (SCE) were used as working, auxiliary and reference electrodes. The 1 cm^2 working electrode was employed for the corrosion studies, and 0.2 g l^{-1} of ammonium sulfate ($(NH_4)_2SO_4$) solution was used as the corrosive media. The coated specimens with a 1 cm^2 exposure area were immersed in the corrosive media for about 1 h prior to impedance and polarization measurements to ascertain the steady-state potential or open circuit potential (OCP). The impedance measurements were carried out in the frequency range 10 mHz–100 kHz at six points per decade frequency with a sinusoidal signal amplitude of 5 mV. The measured EIS data were curve fitted and analyzed with the help of ZsimpWin 3.21 software to obtain impedance parameters. Each experiment was carried out in triplicate and the average values were reported.

3. Results and discussion

3.1. Deposition and morphology of Zn and Zn-Ti O_2 coatings

The deposition of the Zn and Zn-TiO_2 composites were obtained on a mild steel specimen. For pure Zn deposition the steel specimen and a 4 × 4 cm^2 Zn plate were used as cathode and anode, respectively. The deposit was obtained using a bath (table 1), by applying a 0.03 A cm^{-2} current for 10 min with a solution stirring speed of 400 rpm. The deposit was represented by P_0.

Three bath solutions (table 1), each containing 2, 6 and 10 g l^{-1} of TiO_2, respectively, were prepared and stirred for 24 h for the uniform dispersion of nanoparticles. The Zn-TiO_2

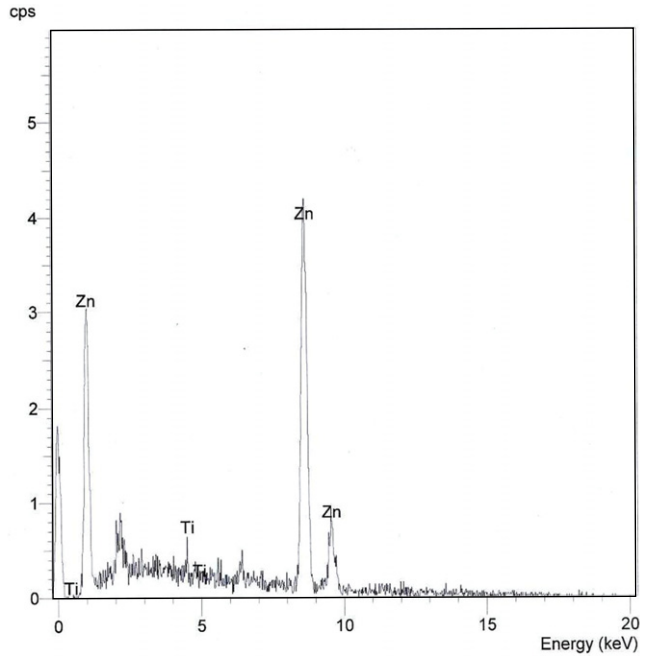

Figure 1. EDS spectra of the P_2 Zn-TiO_2 composite.

composite coatings were obtained on mild steel, and these three coatings were represented as P_1, P_2 and P_3. The EDS spectra for these deposits were recorded and showed the peaks of Ti, revealing the presence of TiO_2 in P_1, P_2 and P_3. The EDS spectra of the P_2 coating is given in figure 1.

The percentage of Ti obtained from the EDS spectra were 0.36, 0.79 and 0.48, respectively, for the P_1, P_2 and P_3 coatings, which were deposited from a plating solution containing 2, 6 and 10 g l^{-1} TiO_2 particles. Among these, the P_2 coating obtained from 6 g l^{-1} TiO_2 nanoparticles exhibited 0.46% Ti, which is slightly higher than the other two coatings (P_1 and P_2).

Further SEM images captured for the composite coatings P_1, P_2 and P_3 confirm the presence of TiO_2 particles in the coated surface. The SEM images of composite coatings showed uniform grains with a more compact crystalline structure when compared to a pure Zn coating. This morphological change is due to the incorporation of TiO_2 particles in the Zn matrix. The morphological changes in the composite coating reveal that the TiO_2 particles deposit in the inner layer of the coating, when compared to the pure Zn coating. The SEM images of all the coatings are shown in figure 2.

To discover the average crystallite size and orientation of crystal planes, XRD patterns for P_0, P_1, P_2 and P_3 coatings were recorded and are shown in figure 3. The average crystallite size for all coatings was calculated from the Scherer equation (1). The average crystallite size of the pure Zn ($P_0 =$ 83.62 nm) coating is less than that of the Zn-TiO_2 composite coatings ($P_1 = 95.85$, $P_2 = 101.32$ and $P_3 = 89.75$ nm). This suggests that the grain size of the Zn crystallites is not refined by the incorporation of TiO_2 nanoparticles, but that the nanoparticles make a compact arrangement of Zn crystallites, which is observed in the SEM images. Note that

$$L = \frac{K\lambda}{\beta \cos \theta}, \tag{1}$$

where K is the Scherer constant, λ the wavelength of scattering, β the full width half maxima, θ the scattering angle and L the average crystal size.

The characteristic peak of TiO_2 in the composite coating was not observed in the XRD patterns, probably due to the small amount of TiO_2 content in composite coating. However, EDS analysis confirmed the existence of TiO_2 particles in the composite coating, which was analyzed by SEM.

To identify the growth of a new crystal plane after the inclusion of TiO_2 particles in the Zn deposit, the texture coefficient was calculated from XRD patterns. The texture coefficient (T_c) was calculated by the equation $T_c = [I_{(hkl)}/\sum I_{(hkl)}] \times [\sum I_{O(hkl)}/I_{O(hkl)}]$ [19], where $I_{(hkl)}$ is the peak intensity of electrodeposits, $\sum I_{(hkl)}$ is the sum of intensities of the independent peaks and O refers to the standard Zn powder sample. The determined texture coefficients are shown in figure 4.

In pure Zn coatings the majority of Zn crystallites are oriented parallel to the (0 0 2), (0 0 4) and (1 1 2) planes. But in composite coatings (P_1 and P_3), the preferential orientation changes to (1 0 1), (1 0 3), (1 1 0) and (1 0 0), (1 0 1), (1 0 2) planes, respectively, with respect to pure Zn coatings. However, deposit P_2 shows a maximum orientation in (1 0 2), (1 0 3) and (1 1 0) planes. These observations suggest that the TiO_2 incorporation changes the preferred orientation pattern, and this change depends on the amount of TiO_2 included in the coating.

3.2. Corrosion behavior of the coatings

The main application of different coatings is in the field of corrosion, where they are employed to obtain good protection against corrosion of the base structure. The protective ability of the coatings was examined by chemical and electrochemical methods. In this study electrochemical methods such as anodic polarization, Tafel plots and impedance measurements were adopted.

3.2.1. Anodic polarization. The anodic polarization behavior of P_0 and P_1 to P_3 coatings was examined in 0.2 g l^{-1} of ammonium sulfate solution in the potential range -1.4 to -0.4 V. The anodic polarization profiles of all coatings are shown in figure 5. The P_0 curve in figure 5 represents the polarization behavior of the bare Zn coating, whereas P_1, P_2 and P_3 represent the polarization behavior of Zn-TiO_2 composite coatings obtained, respectively, from bath solutions containing 2, 6 and 10 g l^{-1} of TiO_2.

The P_1, P_2 and P_3 coatings showed less negative potential for the dissolution of Zn with respect to P_0. Among these, P_2 shows a greater shift of potential towards the less negative direction, which reveals the noble character of the Zn-TiO_2 composite coating, compared to the bare Zn coating. This shift of potential further indicates the high energy requirement needed for the dissolution of Zn from the Zn-TiO_2 composite coating.

The anodic polarization result suggests that the anodic activity of the composite coating is less than that of the pure Zn coating. Hence, this leads to a lower corrosion rate of the composite coating than the bare Zn coating.

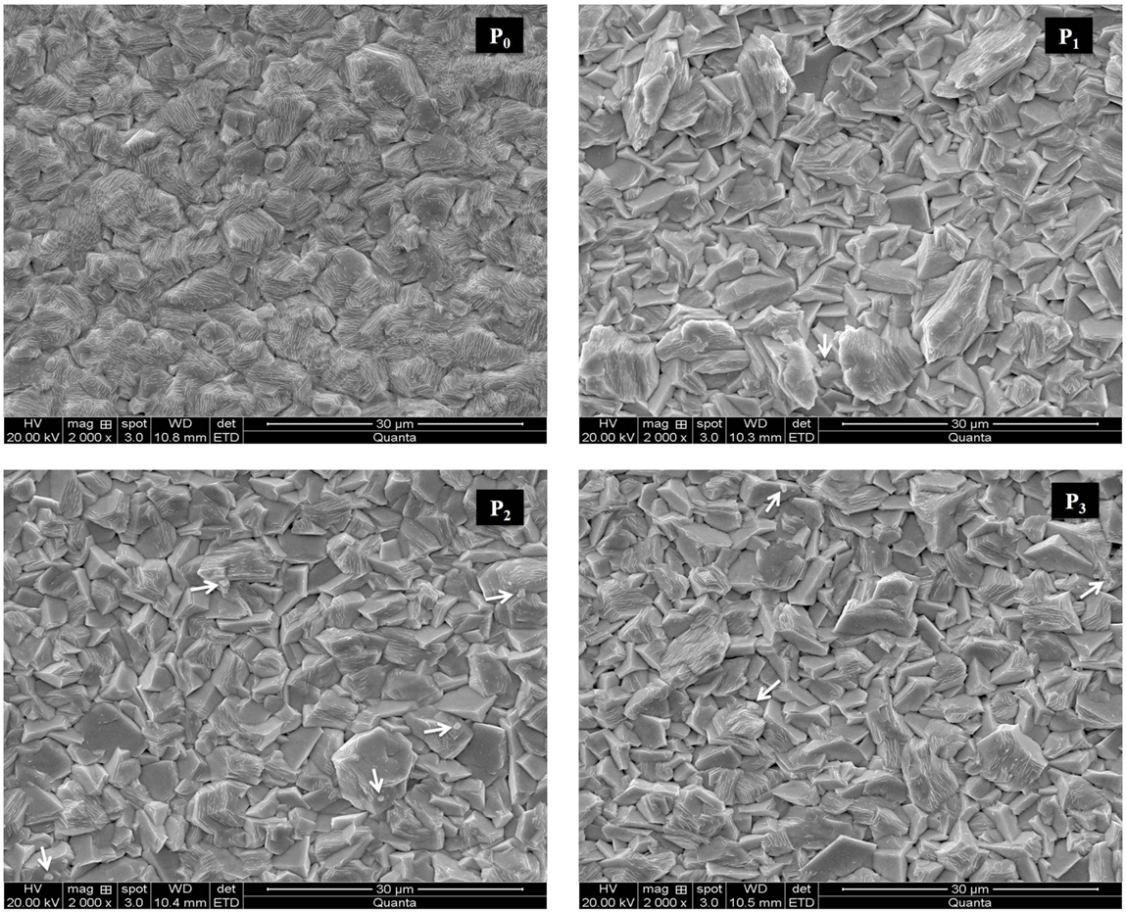

Figure 2. SEM surface morphology of the P_0 Zn coating and the P_1, P_2 and P_3 Zn-TiO_2 composite coatings (the arrows show the presence of TiO_2 particles in the deposit).

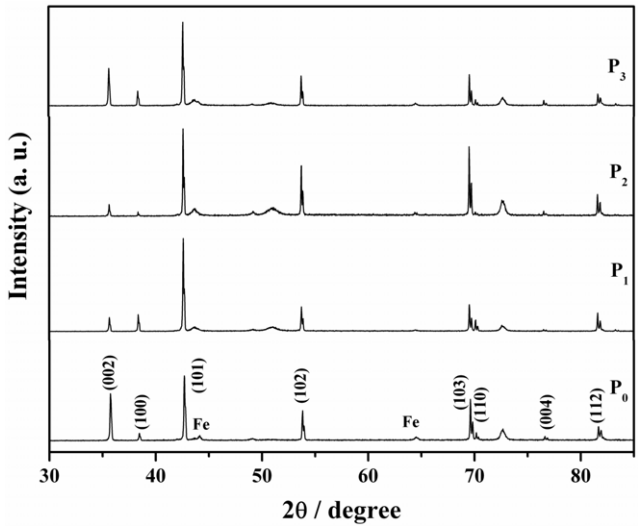

Figure 3. XRD patterns of the P_0 Zn coating and the P_1, P_2 and P_3 Zn-TiO_2 composite coatings.

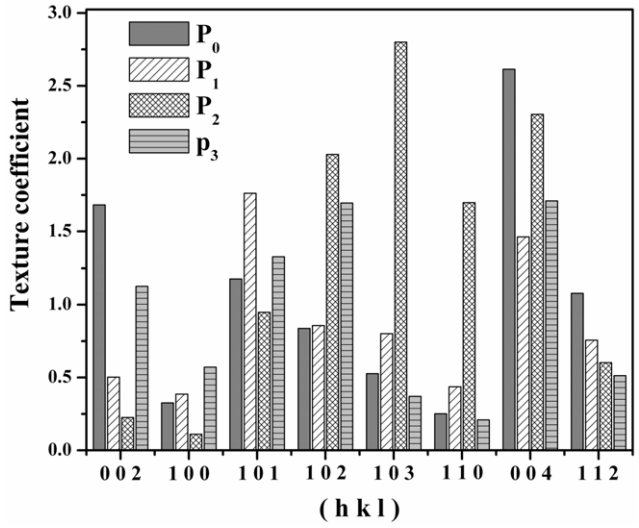

Figure 4. The preferential orientation of the Zn crystallites of the P_0 Zn coating and the P_1, P_2 and P_3 Zn-TiO_2 composite coatings.

3.2.2. Tafel polarization. Tafel plots were used to quantify polarization results and corrosion rate. The plots were recorded in 0.2 g l^{-1} ammonium sulfate solution for different coatings and are given in figure 6. The working electrode was either of pure Zn coating, P_0, or any one of the composite coatings, P_1, P_2 or P_3, and platinum wire and SCE were used as auxiliary and reference electrodes. All the polarization results were measured at the OCP of the respective coatings, and the corrosion parameters of the Tafel measurement are shown in table 2.

The corrosion potential values of composite coatings P_1, P_2 and P_3 were less negative when compared to that of the pure Zn coating, P_0. This shows the noble character of the Zn-TiO_2 composite. The corrosion current for the

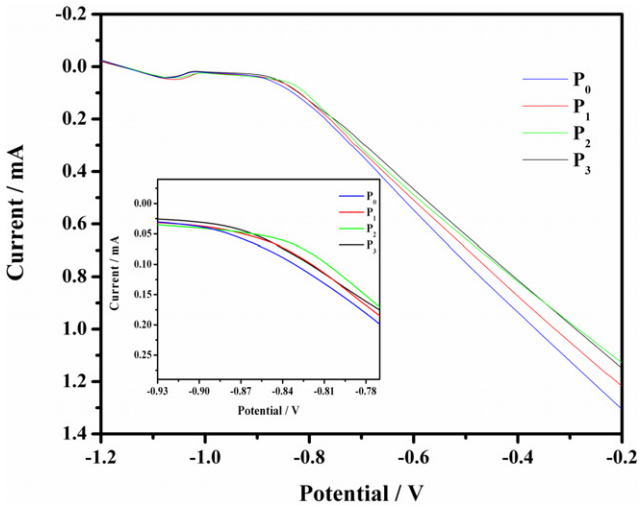

Figure 5. Anodic polarization behavior of the P_0 Zn coating and the P_1, P_2 and P_3 Zn-TiO_2 composite coatings.

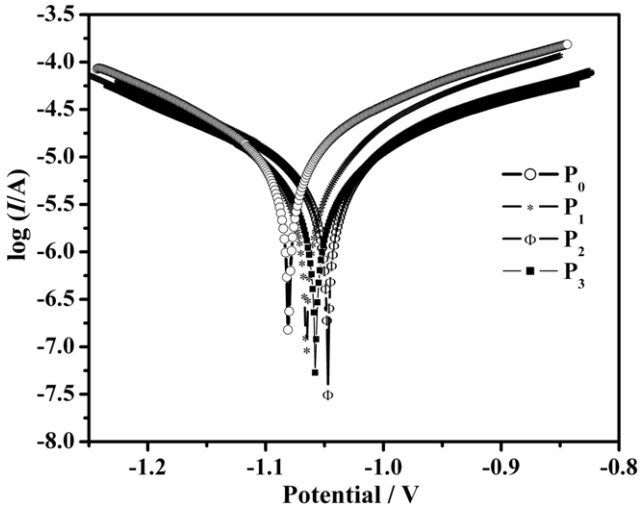

Figure 6. Potentiodynamic polarization curves for the P_0 Zn coating and the P_1, P_2 and P_3 Zn-TiO_2 composite coatings.

P_0 pure Zn coating is 14.09 μA cm^{-2}, whereas the P_1, P_2 and P_3 coatings are 8.947, 7.110 and 8.105 μA cm^{-2}, respectively. In composite coatings, the corrosion current (i_{corr}) is reduced to half that of pure Zn coatings, whereas the value of the corrosion current for P_2 is slightly less than the other composite coatings. This property is imparted by co-deposition of TiO_2 with Zn. It shows that incorporated TiO_2 particles decrease the active surface area in Zn coating responsible for the corrosion process. However, the P_3 coating possesses a higher i_{corr} value with a higher negative corrosion potential value than that of P_2, despite its coating being obtained from a plating bath of higher particle concentration.

The bare Zn coating may possess defects, cracks, gaps, crevices and microholes that are generally larger than micron size. These microholes are the active sites in which the dissolution reaction of Zn takes places during the corrosion process. During electroplating of composite coatings and its consequent growth process, the TiO_2 particles may avoid the formation of these defects by filling the holes.

The kinetic parameters obtained for composite coatings from Tafel plots showed different values when compared to the pure Zn coating. This indicates that incorporated TiO_2 particles in the Zn matrix altered the kinetics of both cathodic and anodic reactions. The E_{corr} and i_{corr} values of composite coatings reveal its anticorrosive property.

Table 2. Electrochemical parameters estimated from potentiodynamic polarization curves.

Specimen	E_{corr} (mV)	i_{corr} (μA cm^{-2})	β_a (mV dec^{-1})	β_c (mV dec^{-1})	Corrosion rate (μg h^{-1})
P_0	−1.081	14.09	207.6	133.2	16.66
P_1	−1.065	8.947	183.8	186.4	10.58
P_2	−1.047	7.110	137.8	146.9	8.408
P_3	−1.058	8.105	235.4	189.21	9.585

3.2.3. EIS studies. The impedance measurement is the most useful and informative method to assess the corrosion behavior of metal coating. Electrochemical impedance measurements are capable of *in situ* and non-destructively probing relaxation phenomena over a wide frequency range. In the present work, the impedance measurement was carried out discontinuously for all coatings at their open circuit potential in the 100 kHz to 10 mHz frequency range. The initially working electrode was left for 1 h to attain equilibrium potential in 0.2 g l^{-1} of ammonium sulfate before making the EIS measurement.

The impedance data are presented as Nyquist plots (figure 7 (P_0) to (P_3)) and typical Bode plots. The Nyquist plots obtained for all coatings with a 1 h immersion period show that P_2 (6 g l^{-1} of TiO_2 particles) has a higher corrosion resistance property than the other coatings. Further, to discover the anticorrosion behavior of coatings exposed to a longer time in the corrosive media, the EIS measurement was carried out at 4, 24, 48 and 72 h.

The typical Nyquist plots in figure 7 correspond to P_0, P_1, P_2 and P_3 coatings immersed for different times. Two capacitive loops (or time constant), i.e. one small loop at higher frequency and one larger one at lower frequency, are observed in the Nyquist plots for all the coatings exposed for 1 and 4 h immersion. Whereas three capacitive loops are observed for all the coatings exposed for 24, 48 and 72 h, and these three loops are well resolved in the Bode plots. On and after 24 h, a thin corrosion product layer was visually identified on the working electrode surface, and this layer may lead to a change in the EIS behavior of the coating.

Shape analysis of the impedance spectra with the fitted electrical equivalent circuit (EEC) helps to understand the electrochemical process occurring at the surface. This means that obtaining a good fit does not imply that the model used is correct. The shape of the spectra is influenced by the electrochemical process at the surface and/or by the geometric factors of the electrode [20]. Hence to obtain impedance parameters, the experimentally determined EIS data were fitted with a suitable equivalent circuit (which possesses a lower percentage of error), with the help of the ZSimpWin 3.21 software.

The electrochemical equivalent circuit in figure 8(a) was used to fit the EIS data measured for all coatings with a 1 and 4 h immersion period. Similarly, 24, 48 and 72 h impedance data measured for all the coatings were fitted with the EEC, as shown in figure 8(b). To obtain more exact fitting results,

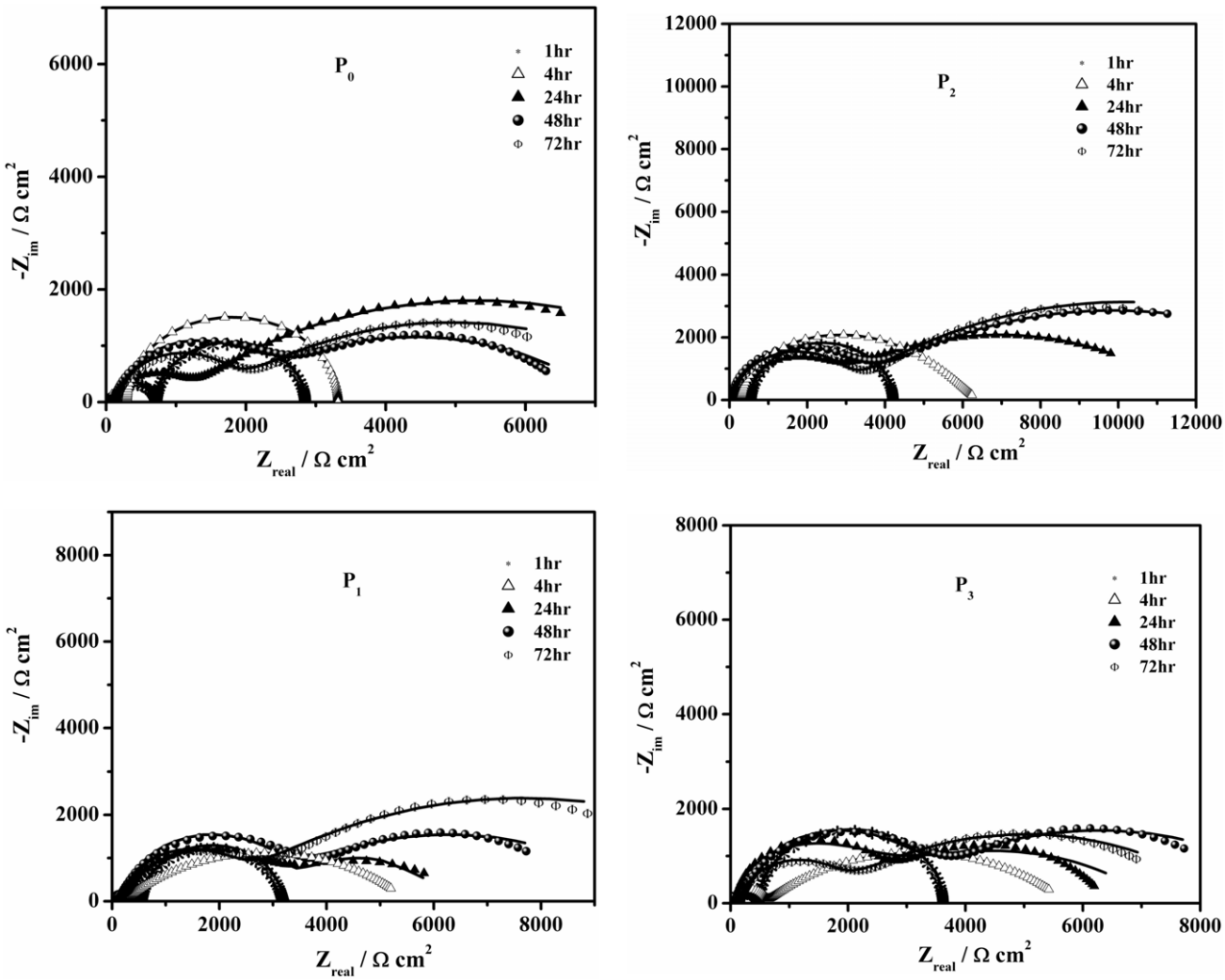

Figure 7. Experimental (—) and simulated (symbols) Nyquist plots of the P_0 Zn coating and the P_1, P_2 and P_3 Zn-TiO_2 composite coatings.

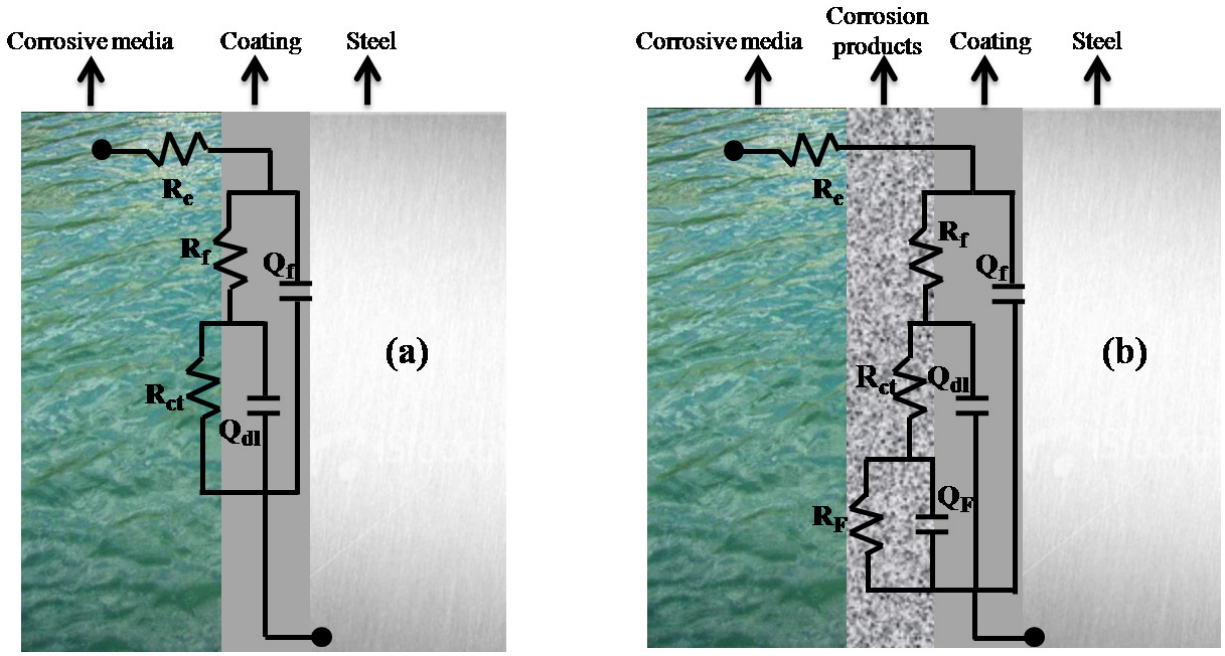

Figure 8. Electrical equivalent circuits used for the simulation of EIS data for the Zn and Zn-TiO_2 composite coatings.

Table 3. Corrosion parameters determined by EEC fitted impedance spectra of Zn and Zn-TiO_2 composite coatings in 2 g l^{-1} of ammonium sulfate solution.

Specimen	Time (h)	Q_f in 10^{-9} (Ω^{-1} cm^{-2} S^{-n})	n_f	R_f (Ω cm^2)	Q_{dl} in10^{-6} (Ω^{-1} cm^{-2} S^{-n})	n_{dl}	R_{ct} (Ω cm^2)	Q_F in 10^{-6} (Ω^{-1} cm^{-2} S^{-n})	n_F	R_F (Ω cm^2)	$^*R_p$ (Ω cm^2)
P0	1	2.88	1	720	9.06	0.832	2130				2850
	4	10.42	1	297	3.84	0.890	3022				3319
	24	123.2	0.956	137	2.73	0.956	1106	300	0.54	5260	6503
	48	335.9	0.887	107	4.68	0.888	2585	247.3	0.614	3600	6292
	72	95.57	0.954	151	5.34	0.928	1917	408.7	0.585	3956	6024
P1	1	4.39	1	521	8.90	0.872	2617				3138
	4	9.36	1	242	6.6	0.781	4956				5198
	24	14.41	1	277	5.312	0.906	3125	243.8	0.541	2417	5819
	48	61.42	0.944	176	8.29	0.893	3454	447.2	0.661	4094	7724
	72	121.1	0.93	127	8.24	0.87	2682	329.1	0.622	6061	8870
P2	1	4.605	1	552	4.623	0.940	3658				4210
	4	5.15	1	411	3.39	0.893	5975				6386
	24	35.35	0.999	166	4.203	1	2836	133.5	0.501	6802	9804
	48	327.8	1	64	2.136	1	3690	208.6	0.501	7510	11264
	72	272.2	0.969	117	2.943	0.919	3417	301.7	0.592	6993	10527
P3	1	7.508	1	484	4.849	0.92	3138				3622
	4	2.84	1	586	3.57	0.87	4834				5420
	24	220.1	1	83	4.054	0.996	2698	191.19	0.688	3413	6194
	48	92.42	0.944	263	5.293	0.893	3582	269.15	0.661	3965	7810
	72	115.5	0.932	138	3.332	0.917	2045	240.4	0.579	4728	6911

$^*R_p = (R_f + R_{ct} + R_F)$.

the capacitance elements (C) in the employed EECs are all replaced by constant phase elements (CPE). The impedance of CPE is defined by the following equation:

$$Z(j\omega) = (Q)^{-1}(j\omega)^{-n},$$

where Q is the CPE constant, j is the imaginary unit, ω the angular frequency ($\omega = 2\pi f$, f is the frequency) and n the CPE exponent ($-1 \leqslant n \leqslant 1$). The CPE exponent n is a measure of capacitance dispersion; for an ideal capacitor $n = 1$ and if there is a decrease in the n value this means that the non-uniform distribution of current arises from surface roughness and surface defects [21–24].

The contribution of each element in circuit 8a (figure 8) is as follows [25, 26].

- R_e is the electrolyte resistance that appears between the reference electrode and the surface of the coated specimen, i.e. the working electrode.
- The high-frequency couple (Q_f–R_f) relates to coating capacitance and coating resistance.
- The low-frequency contribution is attributed to the double layer capacitance (Q_{dl}) with charge transfer resistance (R_{ct}) at the electrolyte/coated surface interface.

In circuit 8b (figure 8), each element is attributed to the following contributions [18], [27–29].

- R_e is the electrolyte resistance that appears between the reference electrode and the surface of the coated specimen, i.e. the working electrode.
- The high-frequency contribution (Q_f–R_f) is ascribed to the dielectric character of the thin surface layer formed from the corrosion products (Q_f) and its electrical leakage from ionic conduction through its pores (R_f).
- The medium-frequency contribution is attributed to the double layer capacitance (Q_{dl}) at the electrolyte/coated surface (Zn and Zn-TiO_2) interface at the bottom of the pores, coupled with the charge transfer resistance (R_{ct}). This charge transfer resistance is closely related to the corrosion rate.
- The low-frequency couple (Q_F–R_F) may relate to a redox process taking place at the surface, likely involving the thin layer of corrosion products accumulated at the electrolyte/working electrode interface.

The calculated impedance data from the equivalent circuit approaches the experimental data of Zn coatings obtained in the absence and presence of TiO_2 particles in the bath solution. The corrosion parameters calculated from the EEC fitted impedance spectra are given in table 3. At 1 and 4 h immersion, there is no considerable corrosion products layer on the electrode surface, hence the obtained response is purely due to the coated surface. As a result, the maximum coating resistance (R_f) with minimum coating capacitance (Q_f) ($Q_f \approx C_f$ since $n \approx 1$, table 3) was observed. Beyond 4 h immersion the Q_f value increases with a decrease in R_f value, because at that time the obtained capacitive behavior is purely due to the dielectric character of the thin formed layer of corrosion products. Hence there may be ionic conduction through the pores layer. Meanwhile, the observed capacitance at the high-frequency range is in nanofarad and suggests a decrease in electroactive area due to the formation of a protective layer, which is confirmed from the mid- and low-frequency responses.

On the other hand, Q_{dl} values decrease with time due to the formation of a slightly thicker layer of corrosion products, which reduces possible contact between the coated surface and the corrosive media, and so the charge transfer resistance increases. Further, the number of electrochemical species available for the oxidation–reduction process become slightly varied, hence the Q_F and R_F values are changed due to the formation and depletion of the corrosion products layer, and the n_F value corresponding to Q_F decreases for all the

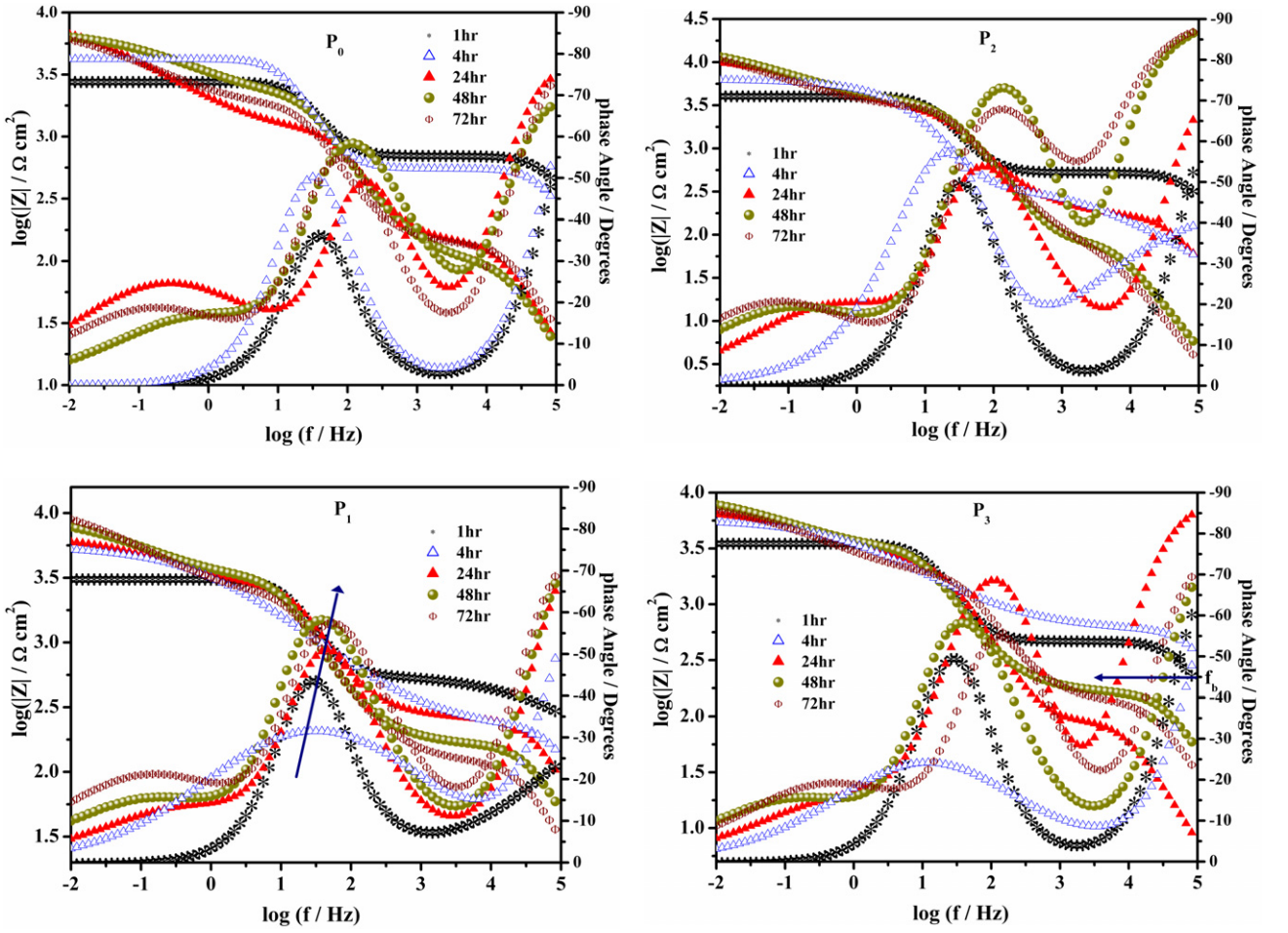

Figure 9. Bode plots corresponding to the P_0 Zn coating and the P_1, P_2 and P_3 Zn-TiO_2 composite coatings.

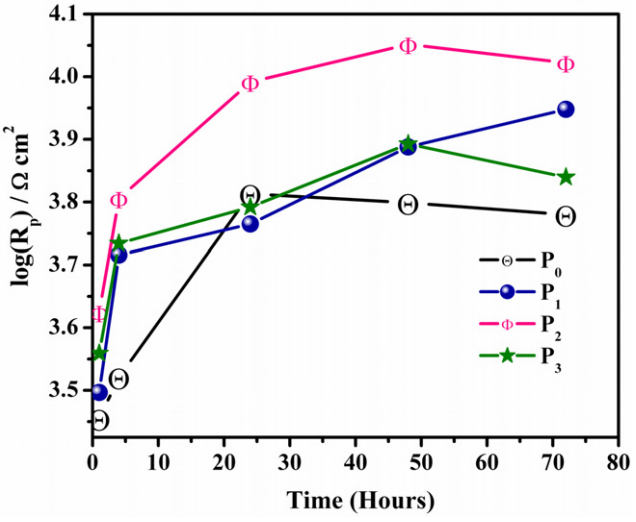

Figure 10. Total polarization resistance value (R_p) with respect to time for the P_0 Zn coating and the P_1, P_2 and P_3 Zn-TiO_2 composite coatings.

coatings. Therefore, surface roughness was created because of the accumulation of a corrosion products layer on the coated surface.

However, R_f and R_{ct} values decrease beyond 4 h of immersion, whereas R_F is high. In spite of this, in the presence of the oxidation–reduction process at the electrode surface, R_p is the parameter most closely related with the corrosion rate [27, 30], and so an increase in R_p values at long immersion times shows the anticorrosive behavior of the coatings.

In the initial EIS measurements, i.e. at 1 and 4 h immersion, the Zn-TiO_2 coatings show a high charge transfer resistance with higher polarization resistance when compared to the pure Zn coating. In particular, the P_2 coating offers high resistance to charge transfer with low double layer capacitance, and also acquires a higher R_p value than the other coating.

EIS measurements for all the coatings at 24, 48 and 72 h show higher R_p values. This may be due to the protective behavior of the formed corrosion products layer in the electrode electrolyte interface. This layer became a barrier for direct contact between the corrosive media and the active electrode surface, which results in a smaller Q_{dl} or C_{dl} (since n_{dl} is nearly equal to 1, hence $Q_{dl} \approx C_{dl}$; see table 3). The coating obtained from 6 g l^{-1} of TiO_2 particles, i.e. P_2, has a smaller Q_{dl} value than the other coatings.

The impedance parameters presented in table 3 and the complex EIS plots confirm that the Zn-TiO_2 coatings obtained from 6 g l^{-1} of anatase TiO_2 particles retain their corrosion resistance properties during up to 72 h of immersion. This means that the P_2 coating gains a higher polarization resistance ($R_p = R_f + R_{ct} + R_F$) than that of other coatings, but the Zn-TiO_2 coating obtained from a higher concentration

of TiO_2, i.e. $10\,g\,l^{-1}$, shows a lower R_p value than the coating obtained from $6\,g\,l^{-1}$ of TiO_2. This may be due to the agglomeration of TiO_2 particles in the plating bath, which leads to a non-uniform distribution of TiO_2 particles in the coating, and is well described by Vlasa *et al* [18]. However, all composite coatings are superior in their anticorrosive property when compared to the P_0 Zn coating.

3.2.4. Analysis of Bode plots. The corrosion behavior of the Zn and Zn-TiO_2 coatings was also analyzed from the Bode plots, i.e. $\log|Z|$ and phase angle (θ) as a function of frequency. Figure 9 (P_0) to (P_3) depicts the Bode plots of the P_0 pure Zn coating and the P_1, P_2 and P_3 Zn-TiO_2 coatings. In Bode plots a low-frequency response is considered a way to explain corrosion resistance properties. The value of $|Z|$ for all the coatings is smallest in 1 and 4 h EIS measurements, but increases in long-term EIS measurements and is shown in figure 9. The Zn-TiO_2 composite coating generated from $6\,g\,l^{-1}$ TiO_2 particles shows a maximum impedance value up to 72 h immersion, when compared to other coatings.

For all the coatings the breakpoint frequency f_b (the frequency for a 45° phase angle; higher frequencies shift correlated with a relative increase in the electrochemically active surface area [31, 32]) shifted towards lower frequencies with respect to time. This indicates that as immersion time increases, the total amount of electrochemically active surface area decreases due to the formation of a protective layer. There is some deviation in f_b shift, and this may be due to a variation in the thickness of the protective layer because of the formation and depletion of corrosive products on the electrode surface. Zn-TiO_2 composite coatings show a maximum shift in f_b towards lower frequency regions when compared to the pure Zn coating, P_0. In particular, the P_2 coating shows a considerable f_b shift towards low frequency.

In the present work an ac circuit, with a parallel resistor and capacitor combination, was employed. Hence, the phase difference that arises between current and voltage leads to current flow through either the capacitor or resistor. The coating is capacitive if resistance and/or capacitance are high, so current mostly passes through the capacitor, and therefore the phase angle would be close to −90°. The coating is resistive if resistance and/or capacitance are low, so current mostly passes through the resistor and the phase angle would be near 0° [25, 33].

A high-frequency response in the Bode plot of phase angle versus log frequency describes the behavior of the coating when it is in contact with corrosive media. EIS measurements for all coatings at 1 and 4 h show the minimum phase angle with less resistance when compared to long-time EIS measurements. There is no considerable corrosion products layer on the coated surface when it is immersed for 1 and 4 h, so ac current mostly passes through the resistor, hence the phase angle is at a minimum. But a considerable adherent corrosion products layer was formed on the coated surface when it was immersed for 24, 48 and 72 h. During long time measurements, the corrosion products layer will be formed between coated surface and corrosive media. This layer acts as an insulator, hence the system behaves like a capacitor. Therefore, the current prefers the capacitor to pass through.

The observed two and three time constants in the Nyquist plots are well resolved in Bode plots of phase angle versus log frequency. The first time constant is in the high-frequency range 10^5 Hz, the second time constant appears between 10^3 and 10^0 Hz, and the third time constant observed for 24 h and beyond, is situated in the low-frequency range 10^{-1} to 10^{-2} Hz.

In the Bode plots, the peak corresponding to the second time constant is considered a characteristic peak for charge transfer resistance. For all coatings in different time measurements, the R_{ct} characteristic peak shifted towards higher frequency with respect to time. This shift shows that as time increases, electron transport between the coated layer and the electrolyte may encounter a longer distance because of the formation of the corrosion products layer [34].

In figure 9 (P_1) and (P_2), the second time constant peak gradually shifted towards higher frequency with respect to time, particularly in the 24, 48 and 72 h measurements. But in other coatings a slight variation in frequency shift is observed. This variation may depend on the thickness of the formed corrosion products layer with respect to time.

All these observations, including the log R_p versus time plot in figure 10, reveal that added TiO_2 particles gave a better corrosion resistance property to the Zn coating. Further, the orientation (1 0 2), (1 0 3) and (1 1 0) intensities are higher for P_2 than P_0, P_1 and P_3. This higher intensity of texture coefficient imparted good corrosion resistance properties to P_2, and similar observations were reported by Mounga *et al* [35]. On the whole, the Zn-TiO_2 composite coating generated from $6\,g\,l^{-1}$ TiO_2 particles shows good anticorrosive behavior to external aggressive environments.

4. Conclusion

A corrosion-resistant Zn-TiO_2 composite coating was successfully generated on steel from a sulfate-chloride Zn plating bath containing $6\,g\,l^{-1}$ TiO_2 nanoparticles. This composite coating showed high corrosion resistance properties with the incorporation of TiO_2 particles. SEM images of the coating exhibited a uniform crystalline arrangement, and SEM and EDS graphs showed the inclusion of TiO_2 particles in the Zn matrix. Further morphological changes in the Zn-TiO_2 composite coating confirm that TiO_2 particles are present in the deposit and cause a perfect crystal orientation with a compact arrangement of Zn crystals. The average crystal size of the coating was 101 nm and rendered the deposit with a compact arrangement. Tafel and linear polarization results revealed that the Zn-TiO_2 composite coating had higher corrosion resistance properties. Impedance data suggested the formation of corrosion products that provided a barrier between coating and corrosive media, and this enabled the deposit to acquire the property of self-protection. This study highlights the use of TiO_2 nanoparticles in generating a Zn-TiO_2 coating that imparts good corrosion resistance to a Zn deposit. The electrolyte could be used to generate Zn-TiO_2 composite coatings on a larger scale.

Acknowledgments

The authors are grateful to the Department of Science and Technology (DST: project sanction no. 100/IFD/1924/

2008–2009, dated 02.07.2008), New Delhi, Government of India, for providing financial assistance, and the Department of Chemistry, Kuvempu University, for providing the laboratory facilities.

References

[1] Prabhu R A, Venkatesha T V, Shanbhag A V, Praveen B M, Kulkarni G M and Kalkhambar R G 2008 *Mater. Chem. Phys.* **108** 283–9
[2] Wang C B, Wang D L, Chen W X and Wang Y Y 2002 *Wear* **253** 563–71
[3] Li J, Sun Y, Sun X and Qiao J 2005 *Surf. Coat. Technol.* **192** 331–5
[4] Wu G, Li N, Zhou D and Mitasuo K 2004 *Surf. Coat. Technol.* **176** 157–64
[5] Thiemig D and Bund A 2008 *Surf. Coat. Technol.* **202** 2976–84
[6] Wang W, Hou F-Y, Wang H and Guo H-T 2005 *Scr. Mater.* **53** 613–8
[7] Balaraju J N, Kalavati and Rajam K S 2006 *Surf. Coat. Technol.* **200** 3933–41
[8] Muller C, Sarret M and Benbella M 2002 *Surf. Coat. Technol.* **162** 49–53
[9] Praveen B M and Venkatesha T V 2009 *J. Alloys. Compounds* **482** 53–7
[10] Praveen B M, Venkatesha T V, Arthoba Naik Y and Prashantha K 2007 *Synth. React. Inorg. Met-Org. Chem.* **37** 461–5
[11] Park J H, Chang W, Byun D and Lee J K 2010 *Phys. Scr.* **T139** 014020
[12] Azizi M, Schneider W and Plieth W 2005 *J. Solid. State. Electrochem.* **9** 429–37
[13] Xiang D and Shan K 2006 *Wear* **260** 1112–8
[14] Shibli S M A, Dilimon V S, Antony S P and Manu R 2006 *Surf. Coat. Technol.* **200** 4791–6
[15] Miller L W, Tejedor-Tejedor M I and Anderson M A 1999 *Environ. Sci. Technol.* **33** 2070–5
[16] Sun B, Reddy E P and Smirniotis P G 2005 *Environ. Sci. Technol.* **39** 6251–9
[17] Linsebigler A L, Lu G and Yates J T Jr 1995 *Chem. Rev.* **95** 735–8
[18] Vlasa A, Varavara S, Pop A, Bulea C and Muresan L M 2010 *J. Appl. Electrochem.* **40** 1519–27
[19] Fustes J, Gomes A and da Silva Pereira M I 2008 *J. Solid. State. Electrochem.* **12** 1435–43
[20] La Mantia F, Vetter J and Novak P 2008 *Electrochim. Acta* **53** 4109–21
[21] Zhang J-T, Hu J-M, Zhang J-Q and Cao C-N 2004 *Prog. Org. Coat.* **51** 145–51
[22] Liu W, Zhang H, Qu Z, Zhang Y and Li J 2010 *J. Solid State Electrochem.* **14** 965–73
[23] Macak J, Sajdl P, Kucera P, Novotny R and Vosta J 2006 *Electrochim. Acta.* **51** 3566–77
[24] Mishra A K, Balasubramaniam R and Tiwari S 2007 *Anti-Corros. Met. Mater.* **54** 37–46
[25] Mahdavian M and Attar M M 2005 *Electrochim. Acta* **50** 4645–8
[26] Liu X and Zheng Y G 2008 *Corros. Eng. Sci. Technol.* **43** 87–92
[27] Muresan L, Varavara S, Stupnisek-Lisac E, Otmacic H, Marusic K, Horvat-Kurbegovic S, Robbiola L, Rahmouni K and Takenouti H 2007 *Electrochim. Acta* **52** 7770–9
[28] Dermaj A, Hajjaji N, Joiret S, Rahmouni K, Srhiri A, Takenouti H and Vivier V 2007 *Electrochim. Acta* **52** 4654–62
[29] Kinlen P J, Silverman D C and Jeffreys C R 1997 *Synth. Met.* **85** 1327–32
[30] Epelboin I, Keddam M and Takenouti H 1972 *J. Appl. Electrochem.* **2** 71–9
[31] Scully J R 1989 *J. Electrochem. Soc.* **136** 979–90
[32] Jianguo L, Gaoping G and Chuanwei Y 2005 *Electrochim. Acta* **50** 3320–32
[33] Mahdavian M and Attar M M 2006 *Corros. Sci.* **48** 4152–7
[34] Hsu C-P, Lee K-M, Huang J T-W, Lin C-Y, Lee C-H, Wang L-P, Tsai S-Y and Ho K-C 2008 *Electrochim. Acta* **53** 7514–22
[35] Mouanga M, Ricq L, Doublade J and Bercot P 2007 *J. Appl. Electrochem.* **37** 283–9